Silicon-based Photon Detectors in Particle Physics Experiments

Lorenz Emberger, Frank Simon, Hendrik Windel

Max-Planck-Institut für Physik, Föhringer Ring 6, 80805 München

November 20th 2019

Abstract

Scintillation detectors are an indispensable part of modern detector development throughout various research fields in physics. With the development of low-noise and small scale silicon photomultipliers (SiPM), the combination of these two technologies lead to the development of very compact and cost efficient detector concepts for high energy particle physics experiments. One of these developments is called CLAWS, which is already in use at the Belle 2 experiment at the SuperKEKB collider in Japan. It is designed for the monitoring of background processes induced by particle injection which happens at a rate of 50 Hz.

In this lab course, a CLAWS detector module based on a scintillating plastic tile read out by a SiPM is characterized. After setting up the experiment, the gain and the thermal noise rate of the SiPM is measured. In the next step, a muon telescope made of two CLAWS detectors is used for the rate determination of cosmic muons. Furthermore, the estimation of the average light output, the so-called light yield, of one detector module will be performed. Before carrying out this experiment, the rate and the light yield are estimated theoretically and compared to the measured values. To perform the analysis of the obtained data, documented code snippets written in

the programming language Python using the packages Pandas, Matplotlib and Scipy in a Jupyter notebook are provided, offering sufficient information to perform the analysis of the underlying data. The lab course will take approximately 3 hours, the analysis can be started while waiting for the long term measurement with a duration of about 1.5 h to complete. Knowing a bit of Python or programming in general is beneficial but not mandatory.

How to reach the Max Planck Institute for Physics is shown in Figure 1.

Figure 1: Public transport: From the U-Bahn station *Studentenstadt* take one of the red paths drawn into the map. Car: Your favorite maps app can guide you to *Föhringer Ring 6, 80805 Mn̈chen.*

Contents

1 Introduction

In recent years, silicon photomulipliers (SiPMs) [1, 2] became prominent in a wide range of fields. This robust, very compact and lightweight visible light photon sensor is simple to operate even under harsh conditions. It has excellent timing properties down to a few 10 ps, is insensitive to magnetic fields up to several tesla, can be operated at low voltages of around 50 V, has a high photon detection efficiency and a relatively high gain, which simplifies the readout electronics. These reasons led to the rapid adaption of SiPMs in particle physics experiments [3]. Successful first applications in high energy physics, combined with steadily increasing performance and decreasing unit prices have made SiPMs popular also in medical imaging, astroparticle physics and more recently also for LIDAR systems.

The relatively good radiation hardness of SiPMs allows applications in highly irradiated locations such as in particle detectors. In 2006, the CALICE Analog Hadron Calorimeter physics prototype using more than 7,500 sensors, was the first large scale application for SiPMs. The first full detector system in a running particle physics experiment with 56,000 photon sensors saw the first beam in 2010 in the neutrino oscillation experiment T2K. Here, SiPMs are used in various detector systems: electromagnetic calorimeters, scintillator based tracking systems and muon detectors in the near detector system. [3]

The success of the SiPM in particle physics is ongoing. Future experiments and detector upgrades consider or are already using SiPMs in applications in particle identification (Belle II), veto systems (NA62), calorimetry (KLOE, sPHENIX), precision timing systems (CMS Phase II Upgrade, CLAWS - SuperKEKB's Beam Background Monitor) and tracking systems (LHCb).

In this *Advanced Lab Course*, students examine detailed SiPM characteristics and get in touch with the CLAWS beam background monitoring system for SuperKEKB consisting mainly of plastic scintillator detector elements read out with SiPMs.

2 Particle Detection

For the understanding of particle detection several processes need to be understood. In this chapter, underlying physics processes such as the energy deposition of charged particles in thin absorbers are explained, followed by a detailed overview of the detector module used in the experiment.

2.1 Passage of Radiation Through Matter

In the course of this experiment, *cosmic muons* are exclusively used as penetrating particles. Therefore, we further concentrate on *heavy charged particles* and not on *electrons and positrons*. Furthermore, as it will be described in more detail in Section 3, the active area of the detector is the a plastic scintillator tile with the dimension $30 \times 30 \times 3\,\mathrm{mm}^3$. The approximation of particles traversing the tile only perpendicular to its $900\,\mathrm{mm}^2$ sized active area leads to the special case of the passage of radiation through *thin absorbers*.

Charged particles traversing through matter experience two main effects: a loss of energy and a deflection from their incident direction. These effects can be described by the following processes

(i) inelastic collisions with the atomic electrons

(ii) elastic scattering from the nuclei

(iii) emission of Cherenkov Radiation

(iv) nuclear reactions

(v) bremsstrahlung.

The dominant processes are (i) and (ii) and happen multiple times per unit path length resulting in the two observable effects. Less likely but, nevertheless, not negligible processes are (iii) to (v). [4]

2.1.1 Bethe Formula[1]

A formula for the energy loss per path length was first developed by Niels Bohr classically and non-relativistic. Later Hans Bethe developed the formula quantum-mechanically, with correction terms of other authors as shown below:

$$-\frac{dE}{dx} = K\rho\frac{Z}{A}\frac{z^2}{\beta^2}\left[ln\left(\frac{2m_e\gamma^2v^2W_{max}}{I^2}\right) - 2\beta^2 - \delta - 2\frac{C}{Z}\right] \tag{1}$$

with

$K =$	$2\pi N_a r_e^2 m_e c^2$	r_e	classical electron radius
m_e	electron mass	N_a	Avogadro's number
I:	mean excitation potential	Z:	atomic number of absorbing material
ρ:	density of absorbing material	z:	charge of incident particle in units of e
$\beta =$	v/c of incident particle	$\gamma =$	$1/\sqrt{1-\beta^2}$
δ:	density correction	C:	shell correction.
W_{max}:	maximum energy transfer in a single collision		

The mean excitation potential, I, is described by the average orbital frequency $\bar{\nu}$ times the Planck's constant, $\hbar \cdot \bar{\nu}$. In practice, large difficulties in calculating $\bar{\nu}$ are avoided by deriving this quantity from actual measurements of dE/dx [4]. As shown in Figure 2 two correction terms C and δ are important at high and low energies, respectively, and are

[1] Often the formula is named *Bethe-Bloch formula*. Felix Bloch was one among others adding correction terms to the formula developed by Hans Bethe. Following this scheme, for reasons of fairness, this formula should be named after more than two persons making it unhandy to write down in texts. Therefore, *Bethe formula* should be fine.

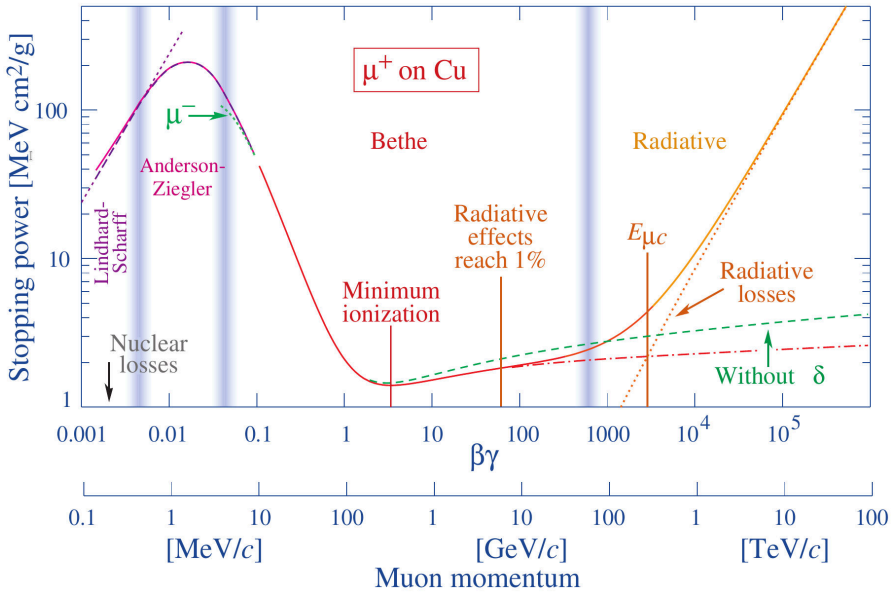

Figure 2: Mass stopping power from positive charged muons in copper. The behavior of muons in plastic scintillator is comparable. At non-relativistic energies, the stopping power is dominated by the $1/\beta^2$ factor with a minimum at $v \simeq 0.96\,c$ [4]. At higher energies, radiative losses become the dominant source of energy transfer. Taken from [5].

not discussed further. As shown in Figure 2, in the region of $0.1 \leq \beta\gamma \leq 100$ ionization is the dominant effect of energy transfer.

The interested reader is is referred to [4] for more detailed information.

2.1.2 Minimum Ionizing Particles

Muons are created as secondary particles when cosmic rays interact with the atmosphere in a height of around 50 km above the surface of the earth. Their major production process is the decay of a charged pion into a muon with same charge and a muon (anti-)neutrino.

$$\pi^{+/-} = \mu^{+/-} + \nu_\mu / \bar{\nu_\mu} \tag{2}$$

Muons reaching the earth's surface have a mean energy of around 4 GeV with a flux $f = 100\,\mathrm{Hz\,m^{-2}}$ for horizontal oriented detectors [5]. Comparing the energy of 4 GeV in Figure 2 it becomes apparent that cosmic muons lie on the plateau located in the middle of the graph making them a natural source of *minimum ionizing particles* or in short: *MIPs*. For this reason, not only experiments in high energy physics benefit from these particles, making them a welcome and universal source for detector calibration.

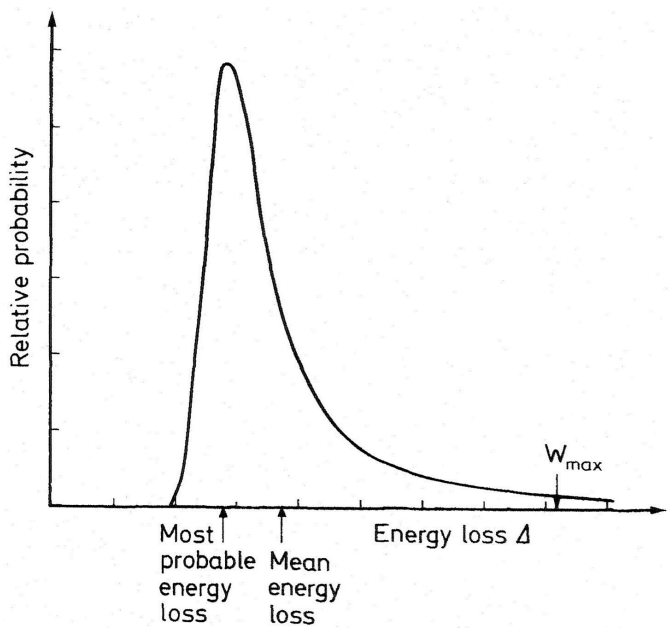

Figure 3: Landau distribution. Typical distribution of energy loss of a traversing particle in a thin absorber. The long tail leads to undefined moments such as mean and variance. Taken from [4].

2.1.3 Thin Absorbers

When a particle passes through an absorbing material, the number of interactions of the incident particle with the surrounding material depends on several properties of the traversed material. For *thin absorbers*, the number of collisions N with the absorbing material is too small for the *central limit theorem*[2] to hold leading to the non-symmetric energy distribution function shown in Figure 3: the *Landau distribution*. The peak of the distribution can be explained by the ionization of the crossing material by the traversing MIPs. The long tail emerges from high energy transfers in single collisions with $\mathrm{W}_{\mathrm{max}}$ as the maximum possible value. The peak of the distribution defines the *most probable* energy loss. The moments mean and variance are analytically undefined, but can be calculated numerically.

[2]"This theorem states that the sum of a large number of random variables is approximately normally distributed, even though the random variables themselves may follow any distribution or be taken from different distributions. [...]" - [6]

3 The CLAWS Detector

Figure 4a shows two CLAWS modules, one without and one with scintillating tile plus additional wrappings. One module consists of a $30 \times 30 \times 3\,\mathrm{mm}^3$ plastic scintillator tile with a bottom mounted SiPM as readout device. The SiPM is housed in a spherical dome (also called dimple) milled into the plastic tile to increase the light collection. Tile and SiPM are mounted on a printed circuit board (PCB) containing electronics such as a pre-amplifier of 19 dB, a differential amplifier of another 12 dB and other. An Ethernet plug delivers three different powers: for the SiPM ($\approx 57\,\mathrm{V}$, $\approx 100\,\mu\mathrm{A}$), the pre-amplifier ($5\,\mathrm{V}$, $\approx 40\,\mathrm{mA}$), and the differential amplifier ($5\,\mathrm{V}$, $\approx 122\,\mathrm{mA}$). The other end of the Ethernet cable is attached to the receiver board (as shown in Figure 4b) transforming the signal back to a single-ended one, amplifying again by 12 dB and forwarding the signal to the data acquisition system (DAQ, see Section 3.2). Furthermore, the receiver board houses a computer steerable power supply transforming a 5 V USB voltage up to 60 V powering the SiPMs.

The active area of the module is the scintillating tile emitting photons when penetrated by a charged particle or high energetic photon. Afterwards, these emitted photons are eventually detected by the SiPM. In order to maximize the detection of emitted photons, the scintillating tile is wrapped in reflective foil. Figure 5 shows the scintillating properties of a plastic scintillator material called *BICRON 408* produced by Saint Gobain. The shielding of photons coming from the ambient light is realized by wrapping the active part in a dedicated black and light-tight aluminum foil as seen in Figure 4a.

3.1 Silicon Photomultiplier

A SiPM is a two dimensional array of 100 to multiple 1000 small *avalanche photo diodes* (APDs) connected in parallel, as shown in Figures 6a and 6b. Therefore, a single APD is also referred to as a pixel in the following.

An APD is a pn-junction with a bias voltage V_{bias} applied in reverse direction creating an electric field which leaves the p-side fully depleted. A SiPM can operate in two modes depending on the value of V_{bias}. Is V_{bias} below the device specific *breakdown voltage* V_{bd} the APD operates in *proportional* mode, where the signal is proportional to the energy of the incoming photon. If V_{bias} exceeds V_{bd}, an avalanche of electron hole pairs is created by an incident photon. Similar to a Geiger-Müller counter, this mode is called *Geiger mode* as shown in Figure 6c. In principle, the avalanche is self-sustaining creating new electron hole pairs as long as $V_{bias} \geq V_{bd}$. For this reason, each pixel is connected in series to a dedicated quenching resistor R_q of $\mathcal{O}(10\,\mathrm{M}\Omega)$, dragging the local V_{bias} below V_{bd} disrupting the avalanche. For the creation of a signal in a single APD, the following sequence takes place:

1. an incoming photon creates an electron hole pair via the photoelectric effect
2. electron and hole are attracted by their corresponding electrode
3. the accelerated charge carriers produce secondary electron hole pairs via the impact

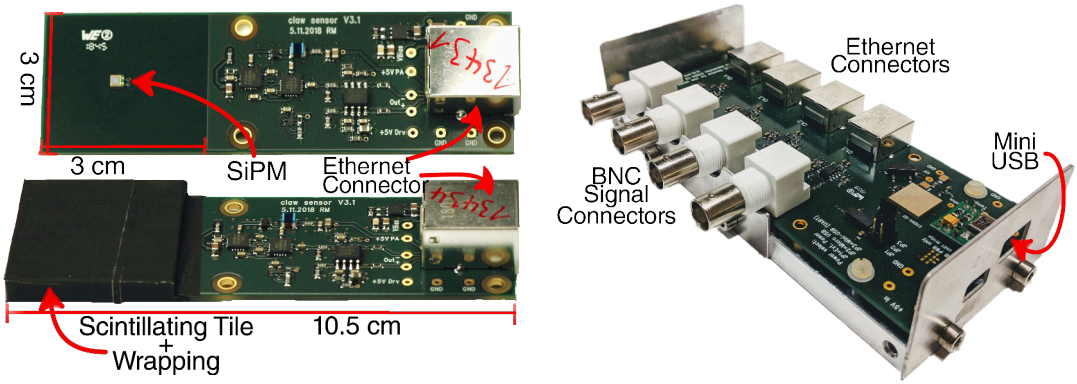

(a) (b)

Figure 4: **(a)** Two CLAWS modules with descriptions of the crucial parts. Top: Bare module without scintillating tile but visible SiPM. Bottom: Fully equipped module. The scintillating tile is wrapped in reflective foil and centered on top of the SiPM. Additionally, the tile is wrapped with light-tight foil to shield ambient light. **(b)** CLAWS receiver board with descriptions of the most needed parts in the lab course. The output signal is send over the BNC signal connectors to the data acquisition system. The mini USB connector allows steering of the board over any standard computer via the Python3 package pyCLAWSps available on GitHub and Python3-pip.

ionization process. This leads to the development of an avalanche of charge carriers in the diode.

4. The current of the electrons in the avalanche leads to a drop of V_{bias} over the quenching resistor. If the number of electrons is high enough, the voltage drops below V_{bd} and the avalanche stops.

Thank to the charge multiplication in the avalanche, the output signal of a SiPM is intrinsically amplified. The so-called *gain* quantifies the amount of charge generated by one photon and is defined by

$$G = \frac{C\,(V_{bias} - V_{bd})}{q}. \tag{3}$$

C is the capacity of one cell of the SiPM, q is the elementary electron charge. By design, the single pixels in a SiPM have approximately the same gain. For this reason, the signal generated by the detection of one photon is constant for a constant bias voltage and called *photon equivalent* (p.e.). If more than one photon is detected, the signal is rising in integer increments of the one p.e. signal. Usual multiplication factors are 10^5 to 10^6 [7].

As every electric device, a SiPM suffers from unwanted side effects, namely *noise*. The most important ones are *thermal dark noise*, *afterpulsing*, and *crosstalk*:

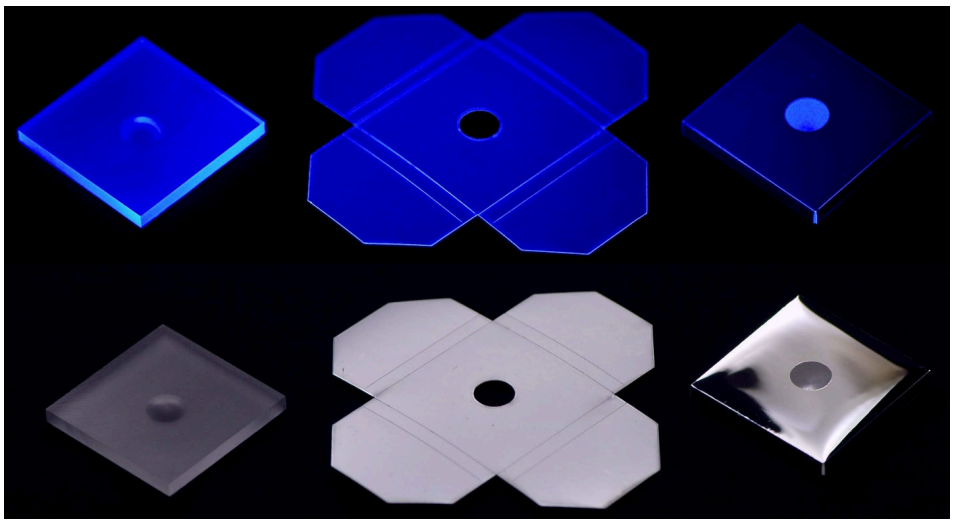

Figure 5: The top and bottom row show the same setting with only one difference: the top row is shined on with artificial UV light, while the bottom row is not. On the left a raw scintillating tile of the material *BICRON 408* is presented. In the middle a laser cut template of the reflective foil is shown. The right side displays a scintillating tile wrapped in reflective foil. The SiPM will sit in the center of the spherical dimple, once the tile is mounted on the PCB.

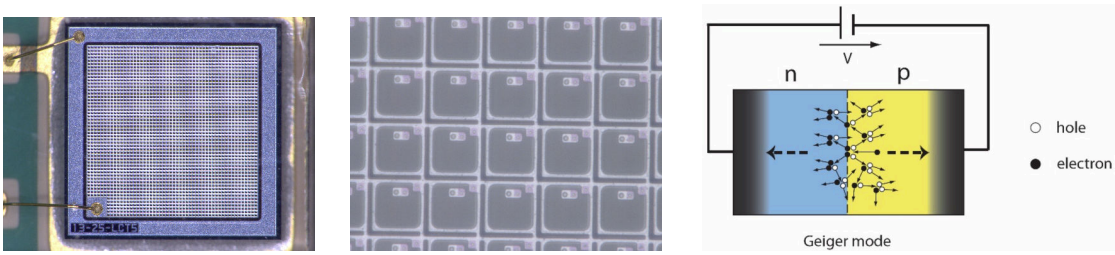

(a) (b) (c)

Figure 6: Different zoom factors of a SiPM. **(a)** Enlarged picture of a Hamamatsu MPPC S13360-1325PE with 25 μm pixel pitch. The active area of the SiPM has the dimensions of $1.3 \times 1.3\,\mathrm{mm}^2$ with 2668 pixels. Photo taken with a microscope at MPP. **(b)** Zoom into active area of the SiPM shown on the left. Single avalanche photo diodes are clearly visible with their sub-components. **(c)** Sketch of a pn-junction with bias voltage applied in reverse. This way the APD works in the Geiger mode producing a very similar signal every time the avalanche is started. Taken from [8].

- **Thermal dark noise** describes the generation of electron hole pairs by thermal excitation which subsequently causes an avalanche. This noise rate scales with the temperature. Typical dark noise rates of SiPMs used in this lab course are around several tens of kHz.

- **Afterpulsing** names an effect caused by trapped charge carriers in an APD triggering a second avalanche after a previous just terminated excitation. This effect can be observed as delayed signals which is not always easy to spot with decreasing afterpulsing rates in recent SiPM generations.

- **Crosstalk** is known as the effect of a photon produced in the recombination of a carrier pair triggering an avalanche in a neighboring pixel.

Further characteristic properties of SiPMs are *cross talk probability*, *photon detection efficiency (PDE)*, *quantum efficiency*, and *breakdown efficiency*:

The *cross talk probability* is defined by the probability of an electron hole pair recombining and emitting a photon times the probability, that an avalanche is triggered by this photon. The *PDE* returns the ratio of the number of detected photons divided by the number of traversed photons as a function of V_{bias} and the wavelength of the impinging photon. Typical values can go up to 50 % for certain wavelength [9]. The *quantum efficiency* returns the probability of the creation of an electron hole pair by an photon and is connected to the PDE while the *breakdown efficiency* is the chance of a carrier pair triggering an avalanche. More detailed information of the underlying processes can be found in [7] and [9].

3.2 Other Hard- and Software

Figure 7 shows the interconnections of the DAQ system for this lab course consisting of of a computer controlled digital oscilloscope digitizing the analog signal coming from the SiPMs, and a software to steer the system, configure the trigger settings and save the data to disk. For the measurement of thermal noise a dedicated frequency counter can be connected via the BNC connectors on the receiver board replacing the oscilloscope. The frequency counter can only be steered manually as described below.

The used oscilloscope is a USB connected *PicoScope 6403* from a company called *Picotech*. It has a sampling rate up to 5 GHz and can store up to 512 MSample in its internal memory. The default settings are a sampling rate of 1.25 GHz and a waveform length of 20 ns per division as shown in Figure 8. The dedicated frequency counter is a *Agilent 53230A* with a maximum sampling rate of 20 ps and is provided to perform a thermal dark noise characterization obtaining the rate of noise signals from the SiPM.

In the following paragraphs, detailed explanations of the usage of the oscilloscope software, the command line tool to power the SiPMs, and the manual programming of the steering counter are presented.

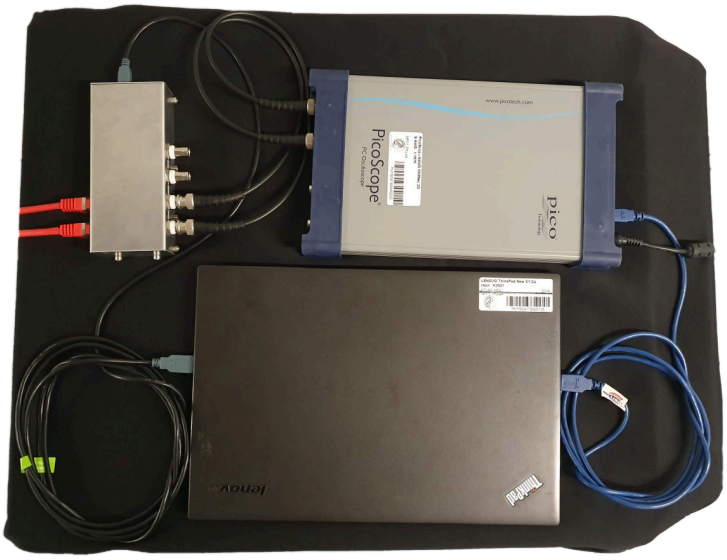

Figure 7: Picture of the interconnections between receiver board (top left), oscilloscope (top right), and lab computer (bottom). The connections between oscilloscope and receiver board use BNC connectors. On the left of the receiver board, two red Ethernet cables connect the Claws modules. Connections from the laptop to the oscilloscope and receiver module use USB cables. A single channel frequency counter is connected to one of the BNC connectors, replacing the PicoScope for one part of the experiment.

Oscilloscope Software The software used in this lab course consists of two components. The first is a commercial software shipped with the oscilloscope *PicoScope 6403* called *PicoScope 6* and is used for steering the oscilloscope and for saving the data.

The configuration of the oscilloscope is done in a *graphical user interface (GUI)* as shown in Figure 8. The provided oscilloscope features 4 input channels for which different signal ranges and coupling modes can be set independently. The trigger can operate in the *Auto* mode ignoring the threshold if the trigger conditions are not met in a defined time, in *Repeat* mode taking a waveform whenever the signal crossed the threshold, and in *Single* mode recording only one waveform. Furthermore, advanced trigger conditions can be set, e.g. to trigger the data taking on coincident signals in two or more channels. Configuring the coincidence trigger, the signals have to satisfy an *and* condition which can be found in the *Logic* tab of the *Advanced Triggers* button in the GUI. The trigger threshold and the used channels are also configured in this tab.

Powering the Sensors The power supply on the receiver board is steered via python in the lab PC's command line. Open a command line and start the python3 interpreter by typing `python`. The python package steering the power supply is called *pyCLAWSps*. Open the web page https://pypi.org/project/pyCLAWSps/ and follow the instructions on how to operate the power supply.

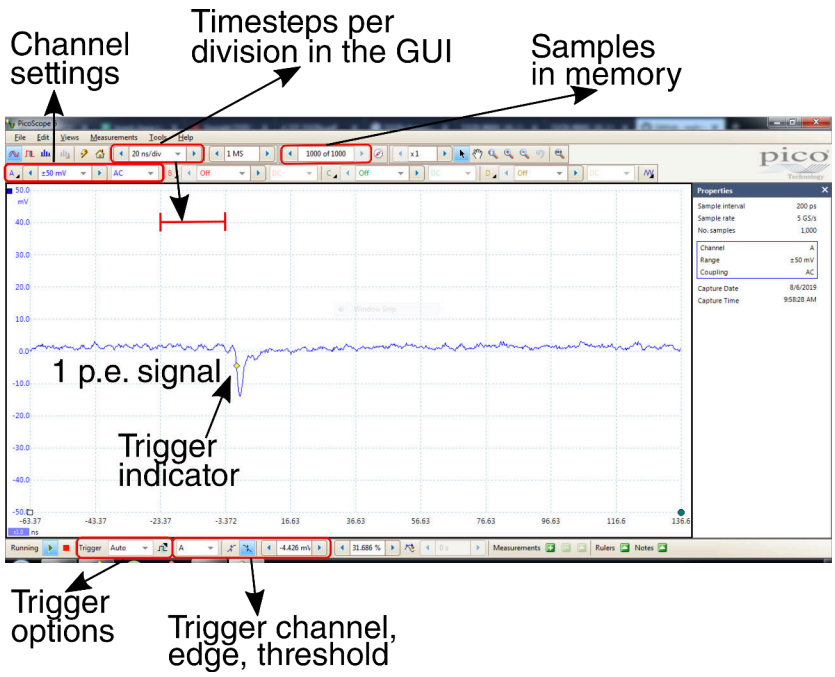

Figure 8: Screenshot of the software to configure the oscilloscope. The waveform is displayed in terms of the voltage reading against the time before and after the trigger threshold (yellow marker) is crossed. The GUI features functionality to activate and deactivate channels, set their voltage range and the coupling mode. The time scale of the waveform display and the sampling rate can be set. The advanced trigger logic is used to implement specific trigger conditions. After configuration, the measurement can be started and stopped with the corresponding buttons.

Steering the Frequency Counter Figure 9 shows the user interface of the frequency counter. This counter is capable of measuring time intervals, frequencies and the total number of counts over a given time interval. In this lab course a measurement is performed to count the amount of thermal dark noise signals in a given time interval. This measurement mode can be selected by the *Totalize* button on the counter. The measurement can be continuous or gated. By setting a gate time, the counter will count for the time set, display the amount of counts and restart the measurement. The gate can be configured with the *Gate* button on the user interface. To only count signals exceeding a given threshold, the totalize measurement has the ability to compare a voltage level to the signal (the *Auto Level* option has to be turned off). In order to trigger on rising or falling slope signals and to set the coupling mode and impedance, the buttons to configure the channel settings are used. They are located above the BNC input connectors on the UI.

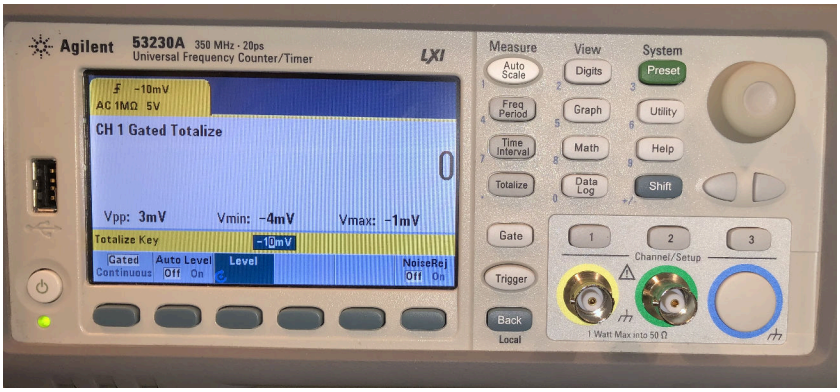

Figure 9: Front face of the frequency counter. The buttons to the right of the display are used to set the measurement mode (Freq/Period, Time Interval or Totalize), gate time and trigger settings. The buttons below the display are used to change the settings of the measurement mode, trigger or gate displayed on the bottom of the display. The buttons above the input BNC connectors (1 and 2) are used to configure e.g. the channels coupling, trigger slope or impedance. The arrow buttons and the round knob on the top right are used to change numerical settings like trigger thresholds or gate time.

4 Experiment

In the course of this experiment, a detailed study of several SiPM characteristics such as the measurement of thermal noise and the determination of the breakdown voltage, as mentioned in Section 3.1 on page 7 will be examined. Finally, the most probable light-yield for one CLAWS module will be determined using a cosmic muon telescope setup and compared to a theoretically obtained value.

4.1 Setting up the Experiment

Power the PicoScope and connect it to the lab PC and open the *PicoScope6* software. If no pop-up window shows up, the oscilloscope is recongnized correctly by the software. Use the description of the CLAWS detector to build a setup capable of powering and reading out one module. Power the sensors with 57.3 V as explained in 3.2. Activate the channel with the connected sensor in the PicoScope software, the coupling is AC, the vertical range should be set to $\pm 50\,\mathrm{mV}$ and the horizontal to $20\,\frac{\mathrm{ns}}{\mathrm{div}}$. Check the presence of the 1 p.e. and 2 p.e. signals by moving the yellow dot in the GUI representing the trigger threshold.

4.2 Gain V_{bias} Correlation

As written in Section 3.1, the gain of a SiPM is a crucial parameter and important for the success of the SiPMs in today's technology. In the following, we will record data and save it in the *.csv* format and extract the gain using *Python3* in a *Jupyter Notebook* with the *Pandas, Numpy & SciPy* packages.

Task Plot the bias voltage V_{bias} dependence on the gain and determine the break down voltage V_{bd}.

1. Record and save 1000 waveforms of each a 1 p.e. and a 2 p.e. signal with the PicoScope software as shown in Figure 8. The number of samples can be adjusted under *Tools* → *Preferences*. Saving the data can be done under *File* → *Save As...* picking location and the .csv format.

2. Repeat step 1 for a reasonable amount of times until you have enough data points for your purpose.

3. **This part should be done after starting 4.4.2, because this measurement requires some waiting time.** In the first step, the waveforms need to be pedestal corrected. Second, obtain the integral of the cleaned waveforms and display the values of the integrals of the 1 and 2 p.e. waveforms in a histogram. Now, the gain can be determined by the difference of the two peaks, referencing the 1 and 2 p.e. signals. To start with this calculation, open the browser and go to the Jupyter tab, where you will find additional instructions.

4.3 Dark Rate Measurement

A low dark rate is important to distinguish real signals from noise. If the dark rate suppresses relevant signals is investigated in the following.

Task Plot the dark rate vs. threshold voltage using the counter for data collection. Therefore, switch on the counter, wait until the loading screen disappears and press the setup button for channel 1. On the bottom of the display, set the coupling to AC, the impedance to $1\,\mathrm{M\Omega}$ and the trigger slope to *negative*. According to the description in 3.2, set the counter to gated totalize with a gate time of 1 second and a trigger level of $-7\,\mathrm{mV}$ (Why?). Disconnect one CLAWS sensor from the PicoScope and connect it to channel 1 of the counter. Record the count rate displayed on the display. Decrease the trigger level step by step until $-35\,\mathrm{mV}$ and record the count rate for each step. Calculate the probability for one fired pixel exciting a neighboring one known as the so-called *cross talk probability* as it is explained in Section 3.1.

Hint Plotting the data on a log-y axis might help understanding. Using python with the matplotlib library in the Jupyter notebook will do the job.

4.4 Light Yield

The light yield of a sensor module is a sensitive parameter making the sensor more or less robust against high dark rates. The light yield is defined as the most probable value of the distribution of fired pixels per traversing MIP (energy distribution) as shown in Section 2.1.3. The higher the light yield, the higher is the efficiency of the sensor system to detect the scintillation light. Ideally, the light yield is larger than the thermal noise. This implies, that the trigger threshold can be increased suppressing noise counts, while still being sensitive real signal events. On the other hand, a high light yield can limit the detectable particle rate if the input dynamic range of the DAQ is scaled too small.

4.4.1 Theoretical Calculation

Task From the most probable energy loss of a muon in the sensor, estimate the number of scintillation photons created.

From the table in Figure 10 obtain the **Bethe ionisation energy loss** of muons in plastic. Compared to the most probable value in figure Figure 3, the Bethe loss is about 1.62 times higher for a PVT based scintillator [5]. From the most probable value, obtain the deposited energy in a 3 mm thick scintillator tile (assume the plastic density $\rho \approx 1\frac{\mathrm{g}}{\mathrm{cm}^3}$). The efficiency of the conversion of deposited energy to photons is about 3%. Calculate the number of scintillation photons in the tile. Assuming a simplified setup with the SiPM attached to one side of an **unwrapped** CLAWS scintillator tile (not in the dimple as in the actual setup), calculate the number of photons reaching

TABLE III-9. Muons in Polyvinyltoluene $[2\text{-}CH_3C_6H_4CHCH_2]_n$

$\langle Z/A \rangle$	ρ [g/cm^3]	I [eV]	a	$k = m_s$	x_0	x_1	$\overline{C}$	δ_0
0.54141	1.032	64.7	0.16101	3.2393	0.1464	2.4855	3.1997	0.00

T	p [MeV/c]	Ionization	Brems	Pair prod	Photonucl	Total	CSDA range [g/cm^2]
		[MeV cm^2/g]					
10.0 MeV	4.704×10^1	7.917				7.917	7.062×10^{-1}
14.0 MeV	5.616×10^1	6.171				6.171	1.285×10^0
20.0 MeV	6.802×10^1	4.816				4.816	2.398×10^0
30.0 MeV	8.509×10^1	3.734				3.734	4.789×10^0
40.0 MeV	1.003×10^2	3.187				3.187	7.707×10^0
80.0 MeV	1.527×10^2	2.388				2.388	2.266×10^1
100. MeV	1.764×10^2	2.237				2.237	3.134×10^1
140. MeV	2.218×10^2	2.082				2.082	4.997×10^1
200. MeV	2.868×10^2	1.992				1.992	7.955×10^1
300. MeV	3.917×10^2	1.957			0.000	1.957	1.303×10^2
325. MeV	4.171×10^2	1.956			0.000	1.956	*Minimum ionization*
400. MeV	4.945×10^2	1.962			0.000	1.962	1.814×10^2
800. MeV	8.995×10^2	2.033	0.000		0.000	2.034	3.817×10^2
1.00 GeV	1.101×10^3	2.066	0.000		0.000	2.067	4.793×10^2
1.40 GeV	1.502×10^3	2.120	0.000		0.001	2.121	6.702×10^2
2.00 GeV	2.103×10^3	2.179	0.000	0.000	0.001	2.181	9.489×10^2
3.00 GeV	3.104×10^3	2.246	0.001	0.001	0.001	2.249	1.400×10^3
4.00 GeV	4.104×10^3	2.293	0.001	0.001	0.002	2.297	1.840×10^3
8.00 GeV	8.105×10^3	2.400	0.003	0.003	0.004	2.410	3.534×10^3
10.0 GeV	1.011×10^4	2.433	0.004	0.004	0.005	2.445	4.358×10^3
14.0 GeV	1.411×10^4	2.480	0.006	0.006	0.007	2.499	5.975×10^3
20.0 GeV	2.011×10^4	2.528	0.009	0.010	0.009	2.557	8.347×10^3
30.0 GeV	3.011×10^4	2.580	0.015	0.018	0.014	2.627	1.220×10^4
40.0 GeV	4.011×10^4	2.615	0.021	0.027	0.018	2.681	1.597×10^4
80.0 GeV	8.011×10^4	2.697	0.048	0.065	0.035	2.845	3.043×10^4

Figure 10: Energy loss of muons in PVT for different energies and interactions. In the top row $\langle Z/A \rangle$ denotes the mean ratio of atomic and mass number, ρ the density, I the mean excitation energy and the parameters a to δ_0 are density effect parameters. In the body of the table, T is the kinetic energy of the muon and p the momentum. The following collumns list the energy loss for different processes. Taken from [10].

the SiPM (area: 1.7 mm × 1.7 mm) from geometrical considerations (the photons are emitted isotropically).

4.4.2 Measurements with the Telescope

Task Take data of cosmic muons and determine the light yield of a CLAWS module.

- Mount two of the CLAWS sensors to the telescope pole as depicted in Figure 11. Make sure that the active areas are as close together as possible and overlap completely. Why is this beneficial for the upcoming measurement?
- Connect the two sensors to channel A and B of the PicoScope. Configure the PicoScope to record coincident signals using the *logic* tab in the advanced trigger

options of the PicoScope software shown in Figure 8. Which threshold might be suitable (think of the dark count rate and estimated number photons)? Why is the coincidence trigger needed?

- Run the measurement for **one hour**. You can work on the analysis of exercise Section 4.2 in the meantime. From the measurement, obtain the light yield of one CLAWS sensor with the provided Jupyter notebook and compare the measured value with the estimated number of photons. Explain possible discrepancies between the two values. How do you interpret the measured muon rate in comparison to the expected rate given in Section 2.1.2?

Figure 11: A picture of the complete telescope setup. The muon sensors are mounted on the pole, the distance between them is adjustable. The Ethernet cables are used to provide power for the sensor and also guides the signal to the oscilloscope. The receiver board features electronics to route the signal from the Ethernet cable to BNC connectors, as well as the power supply. The power supply generates the bias voltage for the SiPMs and is powered via the USB connection. The receiver board is connected to the oscilloscope via BNC to record the signal of the sensors. The USB connection on the oscilloscope is used to configure it and read out the data.

References

[1] V. Golovin and V. Saveliev. Novel type of avalanche photodetector with geiger mode operation. *Nuclear Instruments and Methods in Physics Research Section A: Accelerators, Spectrometers, Detectors and Associated Equipment*, 518(1):560 – 564, 2004. ISSN 0168-9002. doi: https://doi.org/10.1016/j.nima.2003.11.085. URL http://www.sciencedirect.com/science/article/pii/S0168900203029528. Frontier Detectors for Frontier Physics: Proceedin.

[2] D. Renker. Geiger-mode avalanche photodiodes, history, properties and problems. *Nuclear Instruments and Methods in Physics Research Section A: Accelerators, Spectrometers, Detectors and Associated Equipment*, 567(1):48 – 56, 2006. ISSN 0168-9002. doi: https://doi.org/10.1016/j.nima.2006.05.060. URL http://www.sciencedirect.com/science/article/pii/S0168900206008680. Proceedings of the 4th International Conference on New Developments in Photodetection.

[3] Frank Simon. Silicon photomultipliers in particle and nuclear physics. *Nuclear Instruments and Methods in Physics Research Section A: Accelerators, Spectrometers, Detectors and Associated Equipment*, 926:85 – 100, 2019. ISSN 0168-9002. doi: https://doi.org/10.1016/j.nima.2018.11.042. URL http://www.sciencedirect.com/science/article/pii/S0168900218316176. Silicon Photomultipliers: Technology, Characterisation and Applications.

[4] W. R. Leo. *Techniques for Nuclear and Particle Physics Experiments: A How to Approach*. 1987. ISBN 9783540572800.

[5] C. Patrignani et al. Review of Particle Physics. *Chinese Physics C*, 40, 2016. doi: 0.1088/1674-1137/40/10/100001.

[6] W. Krischer R. K. Bock. *The Data Analysis BriefBook (Accelerator Physics)*. Springer, 1998. ISBN 978-3540641193.

[7] Claudio Piemonte and Alberto Gola. Overview on the main parameters and technology of modern silicon photomultipliers. *Nuclear Instruments and Methods in Physics Research Section A: Accelerators, Spectrometers, Detectors and Associated Equipment*, 926:2 – 15, 2019. ISSN 0168-9002. doi: https://doi.org/10.1016/j.nima.2018.11.119. URL http://www.sciencedirect.com/science/article/pii/S0168900218317716. Silicon Photomultipliers: Technology, Characterisation and Applications.

[8] Christian Soldner. *The Time Development of Hadronic Showers and the T3B Experiment*. PhD thesis, Ludwigs-Maximilians-Universität München, 2013.

[9] K. Kobayashi A. Ghassemi, K. Sato. MPPC. Technical report, Hamamatsu Photonics, 2017. URL https://www.hamamatsu.com/resources/pdf/ssd/mppc_kapd9005e.pdf.

[10] Sergei I. Striganov Donald E. Groom, Nikolai V. Mokhov. Muon stopping power and range tables 10 mev–100 tev. *Atomic Data and Nuclear Data Tables*, 78:183–356, 2001. ISSN 0168-9002. doi: https://doi.org/10.1006/adnd.2001.0861.